

Dynamics of an inelastic tagged particle under strong confinement

P. Maynar,^{1,2} M. I. García de Soria,^{1,2} and J. J. Brey^{1,2}

¹⁾*Física Teórica, Universidad de Sevilla, Apartado de Correos 1065, E-41080, Sevilla,*

Spain

²⁾*Institute for Theoretical and Computational Physics. Facultad de Ciencias. Universidad de Granada, E-18071, Granada, Spain*

(*Electronic mail: maynar@us.es)

(Dated: 6 December 2022)

The dynamics of a tagged particle immersed in a fluid of particles of the same size but different mass is studied when the system is confined between two hard parallel plates separated a distance smaller than twice the diameter of the particles. The collisions between particles are inelastic while the collisions of the particles with the hard walls inject energy in the direction perpendicular to the wall, so that stationary states can be reached in the long-time limit. The velocity distribution of the tagged particle verifies a Boltzmann-Lorentz-like equation that is solved assuming that it is a spatially homogeneous gaussian distribution with two different temperatures (one associated to the motion parallel to the wall and another associated to the perpendicular direction). It is found that the temperature perpendicular to the wall diverges when the tagged particle mass approaches a critical mass from below, while the parallel temperature remains finite. Molecular Dynamics simulation results agree very well with the theoretical predictions for tagged particle masses below the critical mass. The measurements of the velocity distribution function of the tagged particle confirm that it is gaussian if the mass is not close to the critical mass, while it deviates from gaussianity when approaching the critical mass. Above the critical mass, the velocity distribution function is very far from a gaussian, being the marginal distribution in the perpendicular direction bimodal and with a much larger variance than the one in the parallel direction.

I. INTRODUCTION

Granular systems are ensembles of macroscopic particles whose interactions are dissipative, in the sense that when two particles (grains) collide, part of the center of mass kinetic energy is transferred to internal degrees of freedom. In the fluid regime, the dynamics of the system (understood as the ensemble of grains independently of their internal structure) can be thought as a sequence of inelastic binary collisions and the system is reminiscent to a molecular gas. A kinetic theory description is applicable in this case¹ and, at a larger scale, hydrodynamics has been shown to describe the macroscopic behavior of the system in many situations, as well as to explain several instabilities that appears in different contexts²⁻⁴.

When energy is continuously supplied to the system, stationary states can be reached in which the energy injected is compensated by the energy dissipated in collisions. The energy injection mechanism can be very simple, for example, by just agitating the box in which the system is, or by vibrating one of the confining walls. Typically, non-homogeneous stationary states are obtained as it can be seen from the hydrodynamic equations². Nevertheless, if the system is agitated vertically and its height is small (of the order of the particles diameter), in such a way that it is quasi-two-dimensional (Q2D), stationary states are reached that can be considered spatially homogeneous⁵⁻⁷. These configurations are specially interesting because, as granular systems are intrinsically out of equilibrium, the generated non-equilibrium homogeneous stationary state can be used to test experimentally many of the out of equilibrium statistical mechanics machinery in a very simple situation. In fact, in the last two decades, a lot of experiments have been performed exploiting the above mentioned property⁵⁻¹⁴. Devices with or without a top lib have been used, being gravity the responsible of the Q2D confine-

ment in the latter case. It is found that, for a wide range of the parameters describing the state of the system, homogeneous stationary states are reached. Nevertheless, by increasing the averaged density or by varying some of the parameters that describe the vibration of the walls, the homogeneous state becomes unstable. Another stationary state is reached in which a dense aggregate, surrounded by a more dilute hotter phase, appears. Let us also mention that, depending on the averaged density, the coexistence is between a solid-like phase and a liquid-like phase⁵ or between a liquid and a gas⁷.

Several models have been proposed in order to explain the above mentioned instability. Particularly interesting is the one introduced in¹⁵ in which the system is modeled as an ensemble of hard disks with a collision rule modified in such a way that, depending on the relative velocity, energy can be gained or lost in a collision. This model has been widely studied finding that the homogeneous stationary state is always stable¹⁶⁻²¹, so that it can not describe the phenomenology seen in the experiments. In order to describe the latter, it appears essential to take into account that energy is injected in the vertical direction and that it is transferred to the horizontal degrees of freedom through inelastic collisions. Although some models have been introduced to incorporate this ingredient²², it seems that the simplest model is an ensemble of inelastic spheres confined between two hard walls and injecting energy through the walls by some mechanism. In Refs.^{23,24} this model was studied assuming that the height of the system is smaller than twice the diameter of the particles (in order to be Q2D), and that the bottom wall is a vibrating elastic sawtooth wall. The top one an elastic wall at rest. It was shown that, for low densities, the pressure in the horizontal direction decays monotonically with the density (apparent negative compressibility) triggering the instability when its horizontal dimension is large enough (otherwise it is killed by heat diffusion). This

is in agreement with the explanation proposed in¹⁵.

In a mixture of two species of grains of equal size but different mass, other new instabilities have been observed. Particularly relevant is the one studied in^{25,26}. Spontaneous segregation shows up with a cluster of heavier particles surrounded by lighter ones. It is found that, when the system is partly segregated, there are sudden peaks of the horizontal kinetic energy of the heavy particles (otherwise small), that partially destroy the cluster. In this paper, we study a mixture of two species of grains of the same size, but in the simpler situation in which there is only one particle of a different mass (the intruder). It is assumed that the bath is dilute and it is always in the homogeneous steady state. In the same lines as in Refs.^{23,24}, the simplest model is considered (neglecting gravity, friction between grains and also friction between grain and the two walls) but, in this case, we will assume that the two walls vibrate. The reason is that, in real experiments, when the system is agitated vertically, both walls inject energy into the system. The objective is to study the dynamics and the stationary states that the tagged particle eventually reaches in the long time limit. Preliminary Molecular Dynamics (MD) results²⁷ have shown that, if the mass of the intruder is close to the one of the bath particles, its distribution function is close to a two-temperatures gaussian, being the horizontal and vertical temperatures of the order of the two bath temperatures. Remarkably, for the parameters considered in²⁷, it was also shown that, when the tagged particle mass was only twice the one of the bath, the vertical temperature was order of magnitudes larger. In addition, the distribution function was not a gaussian anymore. In this paper we will study more deeply these effects by kinetic theory. More precisely, using the same arguments to the ones used to derive the Boltzmann equation for ultra-confined hard spheres^{28,29}, a Boltzmann-Lorentz equation that describes the dynamics of the tagged particle is formulated. In the stationary state, this equation is approximately solved using a two-temperature gaussian ansatz, finding that the vertical temperature diverges for some ‘‘critical’’ value of the tagged particle mass. This critical mass depends on the inelasticity of the particles and on the height of the box. Moreover, if the mass of the intruder is not close to its critical value and it is also smaller than it, MD simulation results show that the gaussian ansatz is a good approximation and a very good agreement with the theoretical prediction is found. This agreement is progressively broken when the mass of the intruder increases and the corresponding critical value is approached (above the critical mass, the distribution function is not gaussian anymore).

The paper is organized as follows: in the following section, the model to be considered is introduced and the Boltzmann-Lorentz equation describing the dynamics of the intruder is formulated. In Sec. III, the dynamics of the intruder is studied assuming that its one-particle distribution function is a two-temperatures gaussian. The properties of the stationary state are also discussed. The theoretical predictions are compared with MD simulation results in Sec. IV, and a good agreement is found in the region of the parameters where the gaussian approximation is fulfilled. The final section of the paper contains a short summary of the results, whose relevance is dis-

cussed. Some details of the calculations are presented in the Appendix.

II. THE MODEL

The system we consider consists of an ensemble of N smooth inelastic hard spheres of mass m and diameter σ , plus another inelastic particle of mass M and the same diameter. Particles are confined between two parallel square-shaped plates of area A , separated a distance h . It is $h < 2\sigma$, so that particles can not jump over each other and the system can be considered to be Q2D. The collision rule between the particle of mass M and the ones of the bath is

$$\mathbf{v}' \equiv b_{\hat{\sigma}} \mathbf{v} = \mathbf{v} + \frac{m}{m+M} (1 + \alpha) (\mathbf{g} \cdot \hat{\sigma}) \hat{\sigma}, \quad (1)$$

$$\mathbf{v}'_1 \equiv b_{\hat{\sigma}} \mathbf{v}_1 = \mathbf{v}_1 - \frac{M}{m+M} (1 + \alpha) (\mathbf{g} \cdot \hat{\sigma}) \hat{\sigma}, \quad (2)$$

where \mathbf{v} and \mathbf{v}_1 are the velocities of the particles of mass M and m respectively before the collision, $\mathbf{g} \equiv \mathbf{v}_1 - \mathbf{v}$, $\hat{\sigma}$ an unit vector joining the two particles at contact from the particle of mass M to the other one, and α the coefficient of normal restitution that will be considered as constant (independent of the relative velocity). It fulfills $0 < \alpha \leq 1$, being $\alpha = 1$ the elastic collision limit. We have also introduced the operator $b_{\hat{\sigma}}$ that transforms the velocities of the particles into the respective velocities after the collision. The collision rule for the particles of the bath is similar, taking $M = m$ and substituting α by the coefficient of normal restitution of the bath particles, α_1 . Periodic boundary conditions are used in the horizontal directions. The bottom and top walls are located at $z = 0$ and $z = h$ respectively and are sawtooth type, i.e. when a particle collides with the bottom (top) wall, the particle always ‘‘sees’’ the wall moving upwards (downwards) with velocity v_0 and undergoes an elastic collision. By introducing the unitary vectors in the direction of the axes $\{\mathbf{e}_x, \mathbf{e}_y, \mathbf{e}_z\}$, the particle-wall collision rules are

$$\mathbf{v} \longrightarrow b_b \mathbf{v} \equiv v_x \mathbf{e}_x + v_y \mathbf{e}_y + (2v_0 - v_z) \mathbf{e}_z, \quad (3)$$

$$\mathbf{v} \longrightarrow b_t \mathbf{v} \equiv v_x \mathbf{e}_x + v_y \mathbf{e}_y - (2v_0 + v_z) \mathbf{e}_z, \quad (4)$$

for the bottom and top wall respectively. We have also introduced the corresponding operators b_b and b_t . Note that this kind of collisions always injects energy into the system and conserve momentum in the direction parallel to the plates. Since momentum is conserved in the collisions between particles, total horizontal momentum is a constant of the motion.

Due to the inelasticity of the particle collisions, stationary states in which the energy lost in collisions is compensated by the energy injected through the walls can be obtained. The stationary states reached by the bath (the actual system *without* the particle of mass M) were studied in^{23,24}, finding that, if the width of the system is small enough, a spatially homogeneous stationary state is reached (in the low density limit the gradients in the vertical direction can be neglected). In the following, we will assume that this is the case. In²³ it was

shown that the distribution function, f_1 , can be accurately approximated by a two-temperature gaussian

$$f_1(\mathbf{v}) = \frac{n_1}{\pi^{3/2} w^2 w_z^2} e^{-\frac{v_x^2 + v_y^2}{w^2} - \frac{v_z^2}{w_z^2}}, \quad (5)$$

where $n_1 = \frac{N}{(h-\sigma)A}$ is the three-dimensional density of the gas. The thermal velocities, w and w_z , are related to the horizontal, T_1 , and vertical, $T_{1,z}$, temperatures through

$$\frac{m}{2} w^2 = T_1, \quad \frac{m}{2} w_z^2 = T_{1,z}. \quad (6)$$

The horizontal and vertical temperatures are defined as usual in kinetic theory

$$n_1 T_1 = \frac{m}{2} \int d\mathbf{v} (v_x^2 + v_y^2) f_1(\mathbf{v}), \quad n_1 T_{1,z} = m \int d\mathbf{v} v_z^2 f_1(\mathbf{v}). \quad (7)$$

The explicit expressions for the steady partial temperatures in terms of the parameters of the bath are²³

$$\gamma_1 \equiv \frac{T_{1,z}}{T_1} = \frac{12(1-\alpha_1) + (5\alpha_1-1)\varepsilon^2}{(3\alpha_1+1)\varepsilon^2}, \quad (8)$$

and

$$T_1 = \left[\frac{6\gamma_1}{\sqrt{\pi}(1+\alpha_1) \left(\gamma_1 - \frac{1+\alpha_1}{2} \right) \varepsilon^3 \tilde{n}_1 \sigma^2} \right]^2 m v_0^2, \quad (9)$$

where the dimensionless height, $\varepsilon \equiv \frac{h-\sigma}{\sigma}$, and the effective two-dimensional density, $\tilde{n}_1 \equiv \frac{N}{A}$, have been introduced. The expression of the temperature given by Eq. (9) differs from the expression given in²³ by a factor 4 because here the two walls are vibrating.

The objective now is to study the dynamics of the tagged particle. It will be assumed that the collisions between the tagged particle and the ones of the bath do not modify the state of the bath. The evolution equation for the one-particle distribution function of the tagged particle, f , immersed in the bath described by the one-particle distribution function, f_1 , follows by the same arguments used to derive the Boltzmann equation for confined systems^{23,28-30} and the following Boltzmann-Lorentz like equation is obtained

$$\left(\frac{\partial}{\partial t} + \mathbf{v} \cdot \frac{\partial}{\partial \mathbf{r}} \right) f(\mathbf{r}, \mathbf{v}, t) = J_z[f_1|f] + L_W f(\mathbf{r}, \mathbf{v}, t). \quad (10)$$

Here J_z is the collisional contribution that takes into account the collisions between the tagged particle and the particles of the bath,

$$J_z[f_1|f] = \sigma^2 \int d\mathbf{v}_1 \int_{\Sigma(z)} d\hat{\sigma} |\mathbf{g} \cdot \hat{\sigma}| [\Theta(\mathbf{g} \cdot \hat{\sigma}) \alpha^{-2} b_{\hat{\sigma}}^{-1} - \Theta(-\mathbf{g} \cdot \hat{\sigma})] f_1(\mathbf{v}_1) f(\mathbf{r}, \mathbf{v}, t), \quad (11)$$

where we have introduced the Heaviside step function, Θ , the operator $b_{\hat{\sigma}}^{-1}$ that replaces all velocities appearing to its right

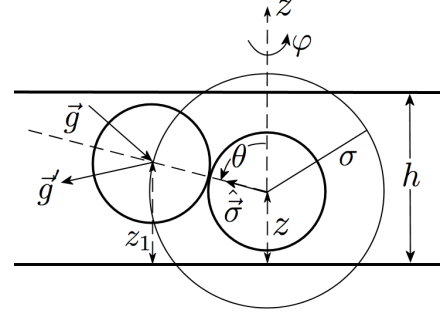


FIG. 1. Collision between the tagged particle and a bath particle. θ and φ are the polar and azimuthal angles respectively.

by the precollisional velocities \mathbf{v}^* and \mathbf{v}_1^* ,

$$\mathbf{v}^* \equiv b_{\hat{\sigma}}^{-1} \mathbf{v} = \mathbf{v} + \frac{m}{m+M} (1 + \alpha^{-1}) (\mathbf{g} \cdot \hat{\sigma}) \hat{\sigma}, \quad (12)$$

$$\mathbf{v}_1^* \equiv b_{\hat{\sigma}}^{-1} \mathbf{v}_1 = \mathbf{v}_1 - \frac{M}{m+M} (1 + \alpha^{-1}) (\mathbf{g} \cdot \hat{\sigma}) \hat{\sigma}, \quad (13)$$

and the region of integration of $\hat{\sigma}$, $\Sigma(z)$, which depends on the confinement. In spherical coordinates, $d\hat{\sigma} = \sin\theta d\theta d\varphi$, where θ and φ are the polar and azimuthal angles respectively (see Fig. 1) and the set Σ can be parametrized as

$$\Sigma(z) = \left\{ (\theta, \varphi) \mid \theta \in \left(\frac{\pi}{2} - b_2(z), \frac{\pi}{2} + b_1(z) \right), \varphi \in (0, 2\pi) \right\}, \quad (14)$$

with

$$b_1(z) = \arcsin \left(\frac{z - \sigma/2}{\sigma} \right), \quad (15)$$

$$b_2(z) = \arcsin \left(\frac{h - z - \sigma/2}{\sigma} \right). \quad (16)$$

Finally, the wall contribution is³¹

$$L_W f(\mathbf{r}, \mathbf{v}, t) = [\delta(z - \sigma/2) L_b + \delta(z - h + \sigma/2) L_t] f(\mathbf{r}, \mathbf{v}, t), \quad (17)$$

with

$$L_b f(\mathbf{r}, \mathbf{v}, t) = [\Theta(v_z - 2v_0) |2v_0 - v_z| b_b - \Theta(-v_z) |v_z|] f(\mathbf{r}, \mathbf{v}, t), \quad (18)$$

$$L_t f(\mathbf{r}, \mathbf{v}, t) = [\Theta(-v_z - 2v_0) |2v_0 + v_z| b_t - \Theta(v_z) |v_z|] f(\mathbf{r}, \mathbf{v}, t). \quad (19)$$

In contrast with the “traditional” Boltzmann-Lorentz equation, the integration in $\hat{\sigma}$ is restricted to $\Sigma(z)$ because, otherwise, the particle of the bath that collides with the tagged particle would not fulfill the constraint of being confined between the two walls.

As in the case of the bath, it is a good approximation to neglect the z dependence of f . Then

$$f(\mathbf{r}, \mathbf{v}, t) \approx f(\mathbf{r}_\perp, \mathbf{v}, t) \equiv \frac{1}{h - \sigma} \int_{\sigma/2}^{h - \sigma/2} dz f(\mathbf{r}, \mathbf{v}, t), \quad (20)$$

where we have introduced the perpendicular component to the z -direction of a vector through $\mathbf{a}_\perp \equiv a_x \mathbf{e}_x + a_y \mathbf{e}_y$. In this situation, by integrating over z in Eq. (10) and replacing $f(\mathbf{r}, \mathbf{v}, t)$ by $f(\mathbf{r}_\perp, \mathbf{v}, t)$ in the collisional operator, J_z , it is obtained

$$\begin{aligned} & \left(\frac{\partial}{\partial t} + \mathbf{v}_\perp \cdot \frac{\partial}{\partial \mathbf{r}_\perp} \right) f(\mathbf{r}_\perp, \mathbf{v}, t) \\ &= \frac{1}{h - \sigma} \int_{\sigma/2}^{h - \sigma/2} dz J_z[f_1|f] + \frac{1}{h - \sigma} (L_b + L_t) f(\mathbf{r}_\perp, \mathbf{v}, t), \end{aligned} \quad (21)$$

that is a closed evolution equation for $f(\mathbf{r}_\perp, \mathbf{v}, t)$. Note that, although the z variable does not appear in Eq. (21), the component v_z still remains.

III. DYNAMICS OF SPATIALLY HOMOGENEOUS STATES

In this section, we will focus on the study of the dynamics of the tagged particle in the most simple situation, in which the system can also be considered spatially homogeneous. In this case, the one-particle distribution function does not depend on \mathbf{r}_\perp and Eq. (21) leads to

$$\frac{\partial}{\partial t} f(\mathbf{v}, t) = \frac{1}{h - \sigma} \int_{\sigma/2}^{h - \sigma/2} dz J_z[f_1|f] + \frac{1}{h - \sigma} (L_b + L_t) f(\mathbf{v}, t). \quad (22)$$

This equation is still difficult to deal with, and we will further assume that f can be approximated by a two-temperatures gaussian distribution, i.e.

$$f(\mathbf{v}, t) = \frac{n}{\pi^{3/2} \Omega(t)^2 \Omega_z(t)^2} \exp \left[-\frac{v_x^2 + v_y^2}{\Omega(t)^2} - \frac{v_z^2}{\Omega_z(t)^2} \right], \quad (23)$$

with $n \equiv \frac{1}{(h - \sigma)A}$. The thermal velocities, $\Omega(t)$ and $\Omega_z(t)$, are related to the horizontal, $T(t)$, and vertical, $T_z(t)$, temperatures through

$$\frac{M}{2} \Omega^2(t) = T(t), \quad \frac{M}{2} \Omega_z^2(t) = T_z(t), \quad (24)$$

where the horizontal and vertical temperatures are defined as in Eq. (7) for the bath

$$nT(t) = \frac{M}{2} \int d\mathbf{v} (v_x^2 + v_y^2) f(\mathbf{v}, t), \quad nT_z(t) = M \int d\mathbf{v} v_z^2 f(\mathbf{v}, t). \quad (25)$$

The validity of the simple ansatz given by Eq. (23) will be confirmed by Molecular Dynamics (MD) simulation results, at least for some range of the system parameters.

Closed evolution equations for the horizontal and vertical temperatures are obtained by taking velocity moments in Eq. (22). For simplicity, we will write the equivalent evolution equations for Ω^2 and Ω_z^2 . By multiplying Eq. (22) by $(v_x^2 + v_y^2)$ and by v_z^2 followed by integrating in the velocity space, it is obtained

$$\frac{d}{dt} \Omega^2 = \mathcal{G}(\Omega^2, \Omega_z^2), \quad (26)$$

$$\frac{d}{dt} \Omega_z^2 = \mathcal{H}(\Omega^2, \Omega_z^2) + \frac{4v_0}{\varepsilon \sigma} \Omega_z^2. \quad (27)$$

The collisional terms are given by

$$\mathcal{G}(\Omega^2, \Omega_z^2) = \frac{1}{(h - \sigma)n} \int d\mathbf{v} (v_x^2 + v_y^2) \int_{\sigma/2}^{h - \sigma/2} dz J_z[f_1|f], \quad (28)$$

$$\mathcal{H}(\Omega^2, \Omega_z^2) = \frac{2}{(h - \sigma)n} \int d\mathbf{v} v_z^2 \int_{\sigma/2}^{h - \sigma/2} dz J_z[f_1|f], \quad (29)$$

and it has been used the exact result derived in³² that establishes that the energy injected by the walls is v_0 times the pressure. Note that, since energy is injected in the vertical direction, collisions with the walls only contribute to the vertical thermal velocity equation. The collisional terms \mathcal{G} and \mathcal{H} are evaluated in Appendix A, obtaining

$$\begin{aligned} \mathcal{G} &= 2\sqrt{\pi} n_1 \sigma^2 \frac{\mu}{\varepsilon} \int_0^\varepsilon dy (\varepsilon - y) (1 - y^2) \\ & \left\{ \mu [(w^2 + \Omega^2)(1 - y^2) + (w_z^2 + \Omega_z^2)y^2]^{3/2} \right. \\ & \left. - 2\Omega^2 [(w^2 + \Omega^2)(1 - y^2) + (w_z^2 + \Omega_z^2)y^2]^{1/2} \right\}, \end{aligned} \quad (30)$$

and

$$\begin{aligned} \mathcal{H} &= 4\sqrt{\pi} n_1 \sigma^2 \frac{\mu}{\varepsilon} \int_0^\varepsilon dy (\varepsilon - y) y^2 \\ & \left\{ \mu [(w^2 + \Omega^2)(1 - y^2) + (w_z^2 + \Omega_z^2)y^2]^{3/2} \right. \\ & \left. - 2\Omega_z^2 [(w^2 + \Omega^2)(1 - y^2) + (w_z^2 + \Omega_z^2)y^2]^{1/2} \right\}, \end{aligned} \quad (31)$$

where the dimensionless parameter

$$\mu = \frac{m}{m + M} (1 + \alpha), \quad (32)$$

has been introduced. The integrals given by Eqs. (30) and (31) can be evaluated exactly, but their expressions are very long and we prefer to leave them in the more compact form given above. Nevertheless, some relatively simpler expressions are obtained for thin systems, by expanding the expressions of \mathcal{G} and \mathcal{H} to second order in ε ,

$$\begin{aligned} \mathcal{G} &\approx 2\mu v \left\{ \frac{\mu}{2} \left[\left(1 - \frac{5}{12} \varepsilon^2 \right) (w^2 + \Omega^2) + \frac{\varepsilon^2}{4} (w_z^2 + \Omega_z^2) \right] \right. \\ & \left. - \frac{\Omega^2}{w^2 + \Omega^2} \left[\left(1 - \frac{\varepsilon^2}{4} \right) (w^2 + \Omega^2) + \frac{\varepsilon^2}{12} (w_z^2 + \Omega_z^2) \right] \right\}, \end{aligned} \quad (33)$$

and

$$\mathcal{H} \approx \frac{\varepsilon^2}{3} \mu v [\mu (w^2 + \Omega^2) - 2\Omega_z^2]. \quad (34)$$

In the above expressions

$$v = \sqrt{\pi} \tilde{n}_1 \sigma (w^2 + \Omega^2)^{1/2}, \quad (35)$$

that, to leading order in ε , is proportional to the collision frequency of the tagged particle.

Eqs. (26) and (27) with \mathcal{G} and \mathcal{H} given by Eqs. (30) and (31) respectively (or their approximate expressions to ε^2 given

in Eqs. (33) and (34) form a closed system of differential equations for the horizontal and vertical thermal velocities. Let us stress that all the dependence in the masses, m and M , and in the inelasticity of the tagged particle, α , in the evolution equations goes through the parameter μ . This is similar to what happens in the non-confined free cooling case³³⁻³⁵. The system of differential equations is highly non-linear, but its structure is clear: the collisions with the walls inject energy in the vertical direction, while the collisions with the bath particles inject/dissipate energy in the vertical and horizontal directions. The collisional contribution to the horizontal thermal velocity is given by \mathcal{G} and, to leading order in ε , it is

$$\mathcal{G} \approx \mathcal{G}_0 = \mu v [\mu(w^2 + \Omega^2) - 2\Omega^2], \quad (36)$$

that is the same as that for inelastic collisions in two dimensions^{34,35}. To leading order in ε , the collisional contribution to the vertical thermal velocity is given by Eq. (34). Its structure is similar to that of Eq. (36), but multiplied by the geometrical factor $\varepsilon^2/3$. This can be intuitively understood as, the thinner the system, the slowest the dynamics of Ω_z is. In addition, Ω is replaced by Ω_z in the “friction” term that leads to equipartition in the elastic case with the elastic walls at rest, i.e. $v_0 = 0$.

Before embarking in the analysis of Eqs. (26) and (27), let us consider a simpler situation which leads to a system of differential equations that can be analytically solved and that will help us to understand many (if not all) features of the general case. If Ω_z/Ω is not very large, \mathcal{G} can be approximated by its leading order in ε contribution, i.e. $\mathcal{G} \approx \mathcal{G}_0$. This simplifies considerably the analysis, as the dynamics of Ω is decoupled from Ω_z within this approximation. It is convenient to introduce the dimensionless thermal velocities

$$X \equiv \frac{\Omega^2}{w^2}, \quad Y \equiv \frac{\Omega_z^2}{w^2}, \quad (37)$$

and the dimensionless time, τ , through

$$d\tau = v dt, \quad (38)$$

that, to leading order in ε , is proportional to the number of collisions the tagged particle experiments in the time interval $(0, t)$. In this time scale, the evolution equations are

$$\frac{d}{d\tau} X = -\mu(2-\mu)X + \mu^2 \quad (39)$$

$$\frac{d}{d\tau} Y = -\frac{2}{3} \left[\mu - \frac{1}{K\sqrt{2(1+X)}} \right] \varepsilon^2 Y + \frac{\mu^2}{3} \varepsilon^2 (1+X), \quad (40)$$

where

$$K(\alpha_1, \varepsilon) = \frac{\gamma_1}{(1+\alpha_1) \left(\gamma_1 - \frac{1+\alpha_1}{2} \right)}, \quad (41)$$

is a function depending on the inelasticity of the particles of the bath, α_1 , and on ε (it does not depend on the inelasticity of the tagged particle, α). Note that, in these units, the dynamics

is independent of the walls velocity and all the dependence on the inelasticity of the bath particles comes through K . Eq. (39) is an inhomogeneous linear equation for X and the time scale in which it evolves is of the order of μ^{-1} . On the other hand, in Eq. (40) Y is coupled with X , but the time scale in which Y evolves is of the order of $(\mu\varepsilon^2)^{-1}$, so that, in this time scale, it can be assumed that X instantaneously reaches its stationary value, X_s , given by

$$X_s = \frac{\mu}{2-\mu}. \quad (42)$$

By substituting X by X_s given by Eq. (42) in Eq. (40), the following approximate equation for Y is obtained

$$\frac{d}{d\tau} Y = -\frac{2}{3} \left[\mu - \frac{(2-\mu)^{1/2}}{2K} \right] \varepsilon^2 Y + \frac{2\mu^2}{3(2-\mu)} \varepsilon^2. \quad (43)$$

If $\mu - \frac{(2-\mu)^{1/2}}{2K} > 0$, Y reaches the following stationary value

$$Y_s = \frac{2\mu^2 K}{(2-\mu)[2\mu K - (2-\mu)^{1/2}]}. \quad (44)$$

Otherwise, Y diverges and there is not a stationary state. Hence, a critical value of μ , μ_c , can be identified as

$$\mu_c = \frac{\sqrt{1+32K^2}-1}{8K^2}. \quad (45)$$

For $\mu < \mu_c$, there is not a stationary state. Note that μ_c depends on ε and the inelasticity of the particles of the bath, α_1 , but it is independent of the inelasticity of the tagged particle. In fact, $\lim_{\mu \rightarrow \mu_c^+} Y_s = \infty$, X_s remaining finite. Equivalently, the critical value of the mass, M_c , above which there is not a stationary state is

$$\frac{M_c}{m} = \frac{(1+\alpha)8K^2}{\sqrt{1+32K^2}-1} - 1. \quad (46)$$

To summarize, the dynamics of the tagged particle in these conditions consists of a fast equilibration in the horizontal direction followed by a slow evolution of Ω_z , that eventually will reach its stationary value if $\mu > \mu_c$. This can be intuitively understood as, for the considered geometry, horizontal collisions (the ones that stabilize Ω) are much more probable than collisions in the vertical direction. The origin of the instability can also be understood. In effect, from Eq. (27) it is seen that the wall contribution is μ -independent, while the collisional contribution increase with μ (consistently with the fact that for more massive tagged particle, less efficient the collisional contribution is). So, for small enough μ the “friction” mechanism is not able to compensate the energy injection and Ω_z diverges.

Let us consider now the general case given by Eqs. (26) and (27) with \mathcal{G} and \mathcal{H} given by their second order in ε expressions (Eqs. (33) and (34)). In this case, if Ω_z^2 is much larger than Ω^2 , as it is the case close to the critical mass, Ω^2 is no longer a fast variable due to the coupling $\varepsilon^2 \Omega_z^2$. This coupling may affect the values of the stationary values as long

as the critical value of the tagged mass. In effect, from Eqs. (26) and (27), the stationary values, Ω_s^2 and $\Omega_{z,s}^2$, fulfill the following set of two equations

$$\mathcal{G}(\Omega_s^2, \Omega_{z,s}^2) = 0, \quad (47)$$

$$\mathcal{H}(\Omega_s^2, \Omega_{z,s}^2) + \frac{4v_0}{\varepsilon\sigma}\Omega_z^2 = 0. \quad (48)$$

Although we are not going to write it explicitly, the dimensionless thermal velocities, X and Y , in the τ scale, also verify a system of differential equations in which v_0 can be scaled. In fact, the system of Eqs. (47) and (48) for the stationary thermal velocities can be transformed in the following one for X_s and Y_s

$$Y_s = \frac{\mu^2(1+X_s)}{2\mu - \frac{\sqrt{2}}{K\sqrt{1+X_s}}}, \quad (49)$$

$$Y_s = \frac{\left[\left(1 - \frac{\varepsilon^2}{4}\right)X_s - \frac{\mu}{2}\left(1 - \frac{5\varepsilon^2}{12}\right)(1+X_s)\right](1+X_s)}{\frac{\varepsilon^2}{4}\left[\frac{\mu}{2}(1+X_s) - \frac{X_s}{3}\right]} - \gamma_1, \quad (50)$$

that leads to a quintic equation that can be solved numerically. For the considered values of the parameters, as in the approximate analysis made before, there is only one physical solution if $\mu > \mu_c$. Moreover, $\lim_{\mu \rightarrow \mu_c^+} Y_s = \infty$, X_s remaining finite. If $\mu < \mu_c$, there is no physical solution. The explicit expression of μ_c for Eqs. (49) and (50) is given by imposing the divergence of Y_s , i.e.

$$\mu_c - \frac{1}{K\sqrt{2(1+X_s)}} = 0, \quad (51)$$

$$\frac{\mu_c}{2}(1+X_s) - \frac{X_s}{3} = 0, \quad (52)$$

whose solution is

$$\mu_c = \frac{\sqrt{9+32K^2}-3}{8K^2}, \quad (53)$$

where K is given by Eq. (41). This expression differs from the approximation obtained previously, Eq. (45), but they agree when the inelasticity of the particles of the bath tends to the elastic limit because $\lim_{\alpha_1 \rightarrow 1} K(\alpha_1, \varepsilon) = \infty$ and $\mu_c \approx \frac{1}{\sqrt{2}K}$ in both cases. The explicit expression of the critical mass in the context of Eqs. (49) and (50) is

$$\frac{M_c}{m} = \frac{8(1+\alpha)K^2}{\sqrt{9+32K^2}-3} - 1. \quad (54)$$

In Fig. 2, μ_c is plotted as a function of the inelasticity of the bath particles, α_1 , for $\varepsilon = 0.5$. The solid line is the theoretical prediction given by Eq. (53) and the (red) dashed line is the approximate expression given by Eq. (45). It is seen that the approximate value is always larger than the exact (up to ε^2 order) value and that both agree in the elastic limit. This can be understood from the fact that, at the critical point, X_s is given by Eq. (52), i.e. $X_{s,c} = \frac{\mu}{\frac{2}{3}-\mu}$, which is larger than the one given by Eq. (42) and which renormalize μ_c into a

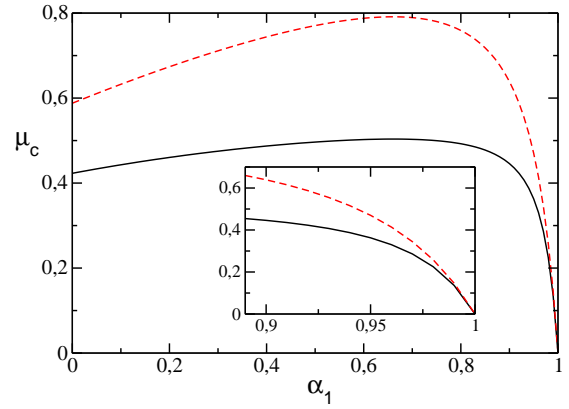


FIG. 2. (Color online) μ_c as a function of the inelasticity of the bath particles, α_1 , for $\varepsilon = 0.5$. The solid line is the theoretical prediction given by Eq. (53) and the (red) dashed line is the approximate expression given by Eq. (45). In the inset, the region close to the elastic limit is shown.

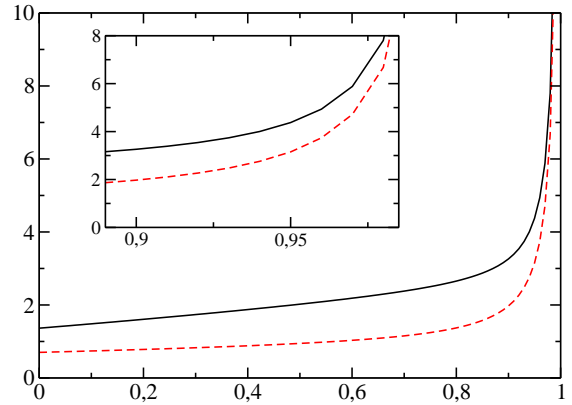


FIG. 3. (Color online) Critical mass as function of the inelasticity for $\varepsilon = 0.5$. It has been considered that $\alpha = \alpha_1$. The solid line is the theoretical prediction given by Eq. (54) and the (red) dashed line the approximate expression given by Eq. (46). In the inset, the region close to the elastic limit is shown.

smaller value. Similar results are obtained for other values of the separation between the walls. To have a clearer physical picture, in Fig. 3, we have plotted the critical mass for $\varepsilon = 0.5$. As this quantity also depends on the inelasticity of the tagged particle, we have considered the case $\alpha = \alpha_1$. The solid line is the theoretical prediction given by Eq. (54) and the (red) dashed line the approximate expression given by Eq. (46). It is seen that the critical mass diverges in the elastic limit but, remarkably, for mild inelasticities, let us say till $\alpha \approx 0.9$, the critical mass is smaller than $3m$, so that the instability is developed “very soon”.

IV. SIMULATION RESULTS

In this section we present MD simulation results of the model introduced in Sec. II in order to compare them with the theoretical predictions obtained in the previous section. The MD simulations are performed using the event-driven algorithm³⁶ taking m , σ and v_0 as units of mass, length and velocity respectively. The used parameters for all the simulations are $N = 585$, $\bar{n}_1 \sigma^2 = 0.06$, and $\varepsilon = 0.5$, varying the tagged particle mass and the coefficients of normal restitution, α and α_1 . The initial condition is generated by putting the particles of the bath with a two-temperatures maxwellian corresponding to the theoretical prediction and the tagged particle at rest. In most of the simulations, the results have been averaged over 20 trajectories. If not, it is explicitly indicated. We have also seen that the bath is always spatially homogeneous and we have controlled if it was disturbed by the presence of the intruder.

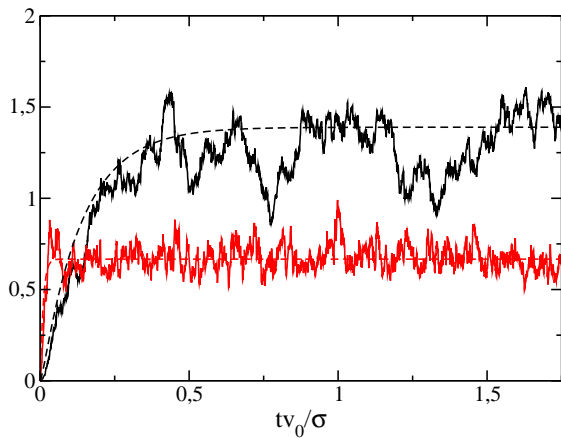


FIG. 4. (Color online) X and Y as a function of the dimensionless time, $v_0 t / \sigma$, for $M = 1.5m$. The (black and red) solid lines are the simulation results for Y and X (respectively) and the (black and red) dashed lines are the (corresponding) theoretical predictions.

In first place, we have considered a system with $\alpha_1 = 0.95$ and $\alpha = 1.0$. For these values of the parameters $\frac{M}{m} \approx 4.5$. In Fig. 4 the dimensionless horizontal and vertical temperatures, X and Y , are plotted as a function of the dimensionless time, $v_0 t / \sigma$, for $\frac{M}{m} = 1.5$. The solid lines are the simulation results averaged over 100 realizations for Y and X . Y reaches a larger stationary value, as expected. The dashed lines are the numerical solution of Eqs. (26) and (27) with \mathcal{G} and \mathcal{H} given by their expression to second order in ε , Eqs. (33) and (34). In this case, if \mathcal{G} is further approximated by \mathcal{G}_0 , an indistinguishable result is obtained. It can be observed that, as discussed in Sec. III, the horizontal temperature reaches the stationary value much quicker than the vertical temperature and that the agreement between the theoretical prediction and the simulation results is remarkably good. In this case, we have also checked that the bath parameters are not disturbed by the presence of the intruder, finding that the distribution function of the bath is approximately a two-temperatures gaussian with

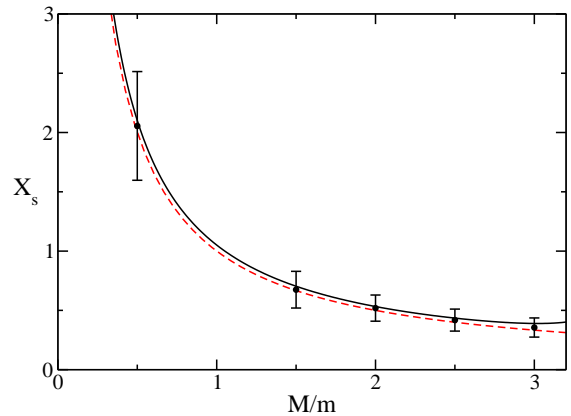


FIG. 5. (Color online) Stationary values of the dimensionless horizontal thermal velocity, X_s , as a function of the dimensionless mass of the intruder, M/m . The points are the simulation results and the solid line the theoretical prediction given by the numerical solution of the system of equations (49) and (50). The (red) dashed line is the approximate solution given by Eq. (42).

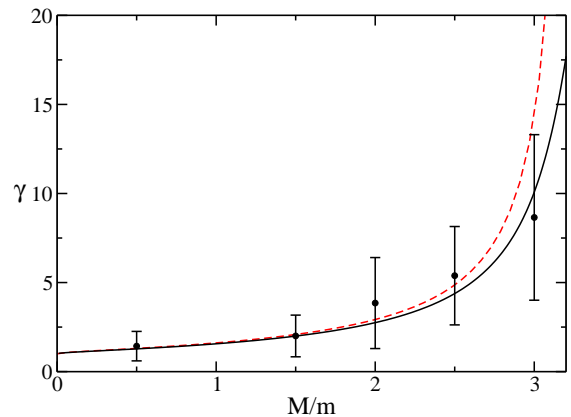


FIG. 6. (Color online) Quotient between the stationary temperatures, $\gamma \equiv \frac{Y}{X}$, as a function of $\frac{M}{m}$. The dots are the simulation results and the solid line the theoretical prediction given by the numerical solution of the system of equations (49) and (50). The (red) dashed line is the approximate solution given by Eqs. (42) and (44)

the measured temperatures in agreement with the theoretical predictions given by Eqs. (8) and (9).

Similar results can be obtained for different values of the tagged particle mass, from which the stationary values of the horizontal and vertical temperatures, as long as their corresponding error bars can be easily measured. In fact, also with $\frac{M}{m} \approx 3.5$, we have seen that the parameters of the bath are not disturbed by the presence of the intruder. For $\frac{M}{m} > 3.5$, the bath velocity distribution function starts deviating from the gaussian and the partial temperatures from their theoretical predictions. In Fig. 5, the dimensionless stationary horizontal temperature is plotted as a function of the dimensionless mass of the tagged particle, $\frac{M}{m}$. The dots are the simulation results and the solid line the theoretical prediction given by the

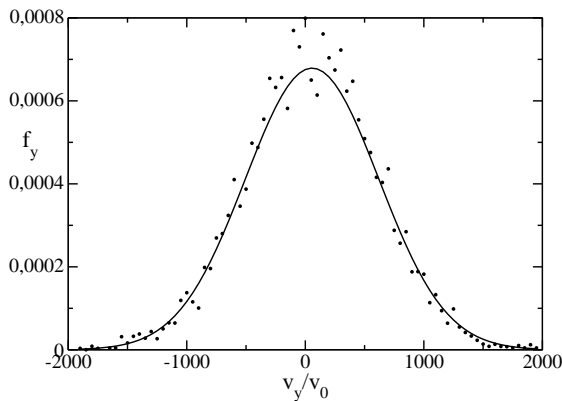


FIG. 7. Normalized marginal velocity distribution in the y direction, f_y , as a function of the dimensionless velocity, $\frac{v_y}{v_0}$, for $M = 4m$. The points are the simulation results and the solid line the gaussian approximation.

numerical solution of the system of equations (49) and (50). The (red) dashed line is the approximate solution given by Eq. (42). It can be seen that the agreement between the simulation results and the theoretical prediction is good, being the two theoretical predictions very similar for $\frac{M}{m} \lesssim 3$. In Fig. 6, the quotient between the stationary temperatures, $\gamma \equiv \frac{Y_s}{X_s}$, is plotted as a function of $\frac{M}{m}$. The dots are the simulation results and the solid line the theoretical prediction given by the numerical solution of the system of equations (49) and (50). The (red) dashed line is the approximate solution given by Eqs. (42) and (44). In this case, for $\frac{M}{m} \approx 3$, there are already some differences between the two theoretical predictions, being the simulation results close to the former, as expected. Again, the agreement between the simulation results and the theoretical prediction is very good.

In the following, we present simulation results for a system with $\alpha = \alpha_1 = 0.98$ where $\frac{M_c}{m} \approx 7.8$. We have performed the same analysis as before, finding similar results³⁷ and we have controlled that the intruder velocity distribution is approximately gaussian. In Fig. 7 the normalized marginal velocity distribution in the y direction, f_y , is plotted as a function of the dimensionless velocity, $\frac{v_y}{v_0}$, for $M = 4m$. The points are the simulation results and the solid line the gaussian approximation. The same is plotted in Fig. 8 but in the z direction. It is observed that the gaussian approximation accurately describes the shape of the marginal distributions, at least for thermal velocities where the data are shown. Similar results are obtain for $M < 5m$. A more quantitative analysis can be carried out by measuring the kurtosis of the marginal distributions

$$a_{2,xy} = \frac{\langle (v_x^2 + v_y^2)^2 \rangle}{2\langle v_x^2 + v_y^2 \rangle^2} - 1, \quad a_{2,z} = \frac{\langle v_z^4 \rangle}{3\langle v_z^2 \rangle^2} - 1, \quad (55)$$

where $\langle \dots \rangle$ means average over different realizations in the stationary state. In Fig. 9, the (black) circles and the (red) squares are the simulation results for $a_{2,xy}$ and $a_{2,z}$ respectively, that are plotted as a function of the dimensionless mass.

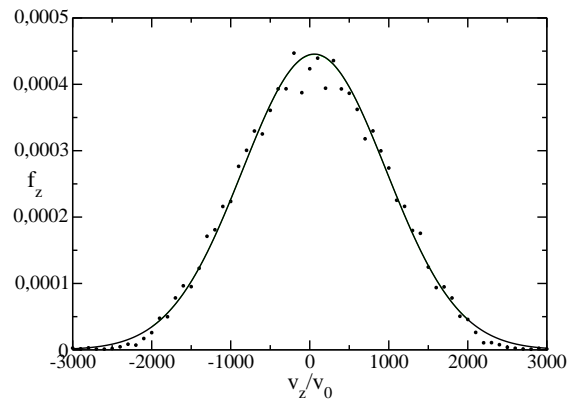


FIG. 8. Normalized marginal velocity distribution in the z direction, f_z , as a function of the dimensionless velocity, $\frac{v_z}{v_0}$, for $M = 4m$. The points are the simulation results and the solid line the gaussian approximation

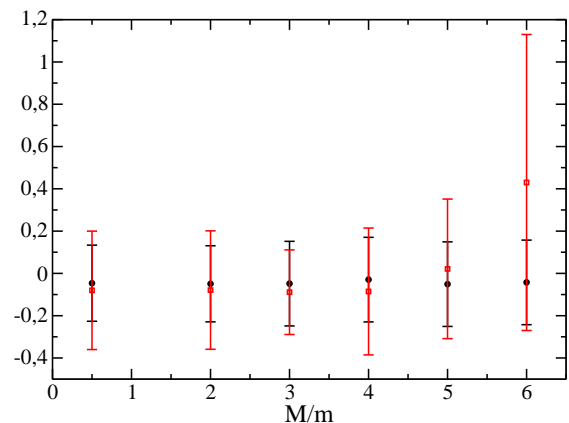


FIG. 9. (Color online) $a_{2,xy}$ and $a_{2,z}$ as a function of the dimensionless mass, $\frac{M}{m}$. The (black) circles are the simulation results for $a_{2,xy}$ and the (red) squares for $a_{2,z}$.

It is observed that $a_{2,xy}$ remains approximately unchanged for the plotted mass values, while $a_{2,z}$ start varying with respect to the small-mass value at $M \approx 5m$, strongly deviating from the gaussian value already for $M = 6$.

We have also investigated the behavior of the system for $M > M_c$ for two different values of the intruder mass, $M = 10m$ and $M = 12m$. We have performed MD simulations, finding that a stationary state is reached in the long time limit. The obtained values for the stationary partial temperatures are $X_s = 1.3 \pm 0.4$ and $\gamma = 570 \pm 260$ for $M = 10m$ and $X_s = 1.9 \pm 0.5$ and $\gamma = 800 \pm 270$ for $M = 12m$. This strong non-equipartition is remarkable as the vertical temperature is nearly three orders of magnitude larger than the horizontal temperature. The measured kurtosis are $a_{2,xy} = 0.1 \pm 0.3$ and $a_{2,z} = -0.48 \pm 0.09$ for $M = 10$ and $a_{2,xy} = 0.1 \pm 0.3$ and $a_{2,z} = -0.52 \pm 0.03$ for $M = 12$, so that the z -marginal velocity distribution is strongly non-gaussian. In Fig. 10, f_z is plotted as a function of $\frac{v_z}{v_0}$ for $M = 10m$, where a bimodal shape is

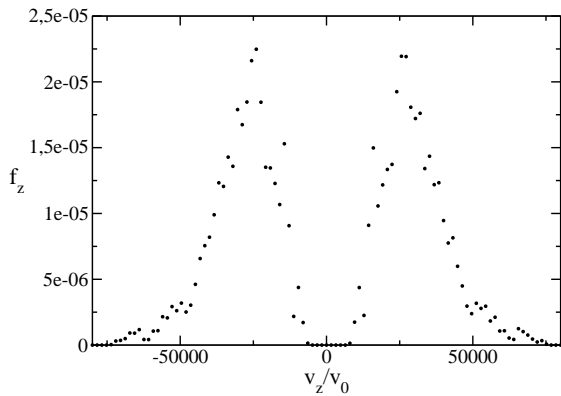


FIG. 10. Normalized marginal velocity distribution in the z direction, f_z , as a function of the dimensionless velocity, $\frac{v_z}{v_0}$, for $M = 10m$.

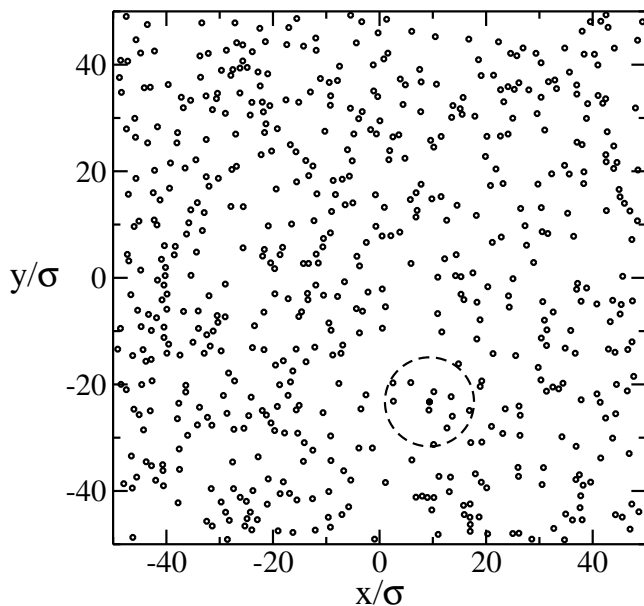


FIG. 11. Snapshot of the system with $M = 10m$. The intruder is in the center of the slashed circle and is represented by a filled symbol.

clearly observed. Similar results are obtained for $M = 12m$. It must be remarked here that the bath velocity distribution function is actually disturbed for the analyzed values of the masses in the $M > M_c$ case. In effect, the bath partial temperatures deviate from the case without the presence of the intruder and the distribution function deviates from the gaussian shape. Concretely, the kurtosis of the bath in the xy direction is 0.3 ± 0.12 and 0.35 ± 0.12 for $M = 10m$ and $M = 12m$ respectively. In the z -direction it is 0.20 ± 0.08 and 0.24 ± 0.07 for $M = 10m$ and $M = 12m$ respectively. In any case, it is expected that, as increasing the number of bath particles, the influence of the intruder in the bath can be minimized. Nevertheless, even in these extreme conditions where the bath is highly disturbed by the intruder, the bath is still spatially homogeneous as can be seen in Fig. 11.

Finally, we have also performed MD simulation in the mass range $6 < \frac{M}{m} < 10$, but no clear conclusions can be extracted from them, even the existence of a stationary state. The closer to the critical mass, the larger the relaxation time to reach the stationary state is, and more expensive simulations are needed to study the behavior of the system with the same degree of accuracy as in the $\frac{M}{m} \leq 6$ and $\frac{M}{m} \geq 10$ cases.

V. CONCLUSIONS AND OUTLOOK

In this paper we have analyzed the dynamics of an intruder, an inelastic hard sphere, immersed in a bath composed of inelastic hard spheres of the same diameter but different mass. The system is confined between two hard parallel plates perpendicular to the vertical direction that inject energy into the system in the direction perpendicular to them. A *critical* intruder mass, M_c , is identified for which the vertical temperature diverges when approaching it from below, remaining the horizontal temperature finite. The mechanism triggering the transition is identified in the context of a very simple model based on the equations for the horizontal and vertical temperatures that are derived from a kinetic theory description under clear and controlled approximations.

In the theoretical study, it is assumed that the bath is in the corresponding spatially homogeneous stationary state and that it is not disturbed by the presence of the intruder. The dynamics of the distribution function of the intruder is given by a Boltzmann-Lorentz-like equation with two kind of collisional terms: one that takes into account the collisions between the intruder and the bath particles and another that takes into account the collisions between the intruder with the hard walls. The former is modified with respect to the non-confined case in order to take into account that only the collisions compatible with the constraints are possible. The kinetic equation is solved for spatially homogeneous states assuming that the distribution function is a two-temperatures gaussian corresponding to the vertical and horizontal temperatures. Under these hypothesis, closed evolution equations for the partial temperatures are obtained. Both equations contain a term that comes from collisions between the intruder and the bath particles that dissipates/injects energy. The energy injection term that takes into account the collisions of the intruder with the walls only appears in the vertical temperature equation, consistently with the fact that the walls inject energy in the vertical direction. The fact that the collision between the particles term is mass-dependent, while the intruder-wall term is mass-independent, makes possible a stationary state only if the intruder mass is smaller than certain *critical* mass, M_c . If $M > M_c$, there is not stationary state in the gaussian approximation and the vertical temperature diverges in the long-time limit.

A very good agreement between the MD simulation results and the theoretical predictions is obtained for $M < M_c$ both, for the dynamics and the stationary values reached in the long-time limit. MD simulations show that the intruder velocity distribution function is, in effect, close to a two-temperatures gaussian if $M < M_c$ and the mass is not too close to the critical mass while, close to the critical mass, the distribution function

is not gaussian anymore. Above the critical mass, the simulation results show that a stationary state is reached but with a vertical temperature orders of magnitude larger than the horizontal temperature and being the partial distribution function in the vertical direction a bimodal distribution. Moreover, MD results also show that the bath is not disturbed by the intruder if $M < M_c$ and M is not close to the critical value, consistently with the theoretical analysis. For M close to the critical mass or $M > M_c$, the distribution function is strongly disturbed and the gaussian approximation fails. Physically, the reason is that, as the vertical temperature of the intruder is so large, there can be collisions between a particle of the bath and the intruder having a extremely high vertical velocity that affect the dynamics of the bath.

The present study opens the possibility of further studies that are under investigation. First, the problem of diffusion. It seems that, in the region where the intruder distribution function is gaussian, we should have normal diffusion. When the distribution function is not gaussian, the situation is not clear. In any case, what it is clear is that the non gaussianities will modify the transport coefficients even if the diffusion is still normal. Second, the microscopic origin of the bimodal distribution. It seems plausible to tackle the problem for very large masses by studying the corresponding Fokker-Planck equation. Finally, taking into account that the microscopic origin of the instability is very general and simple, we think that many of the features studied in the paper could be observed in actual experiments. Although a quantitative agreement of the results reported here with experiments is not to be expected, due to the several simplifications introduced in the theoretical model, e.g. neglecting friction and rotation of the particles, a qualitative agreement looks quite possible, since the elements considered in our description are also present in experiments. In particular, the existence of a *critical* mass for which the vertical temperature diverges when approaching it from below, and the transition from the gaussian distribution to the bimodal distribution above the critical mass.

ACKNOWLEDGMENTS

This research was supported by Consejería de Economía, Conocimiento, Empresas y Universidad de la Junta de Andalucía (Spain) through Grant. US-1380729 and by the Ministerio de Ciencia e Innovación (Spain) through Grant PID2021-126348NB-100 (both partially financed by FEDER funds).

Appendix A: Velocity moments of the collisional term

The objective of this Appendix is the evaluation of the function \mathcal{G} defined in Eq. (30). The evaluation of \mathcal{H} given by Eq. (31) follows similar lines and will not be given. By standard arguments, the expression of \mathcal{G} given by Eq. (28) can be

rewritten as

$$\mathcal{G} = \frac{\sigma^2}{2(h-\sigma)n} \int d\mathbf{v} \int d\mathbf{v}_1 \int_{\sigma/2}^{h-\sigma/2} dz \int_{\Sigma(z)} d\hat{\boldsymbol{\sigma}} f_1(\mathbf{v}_1) f(\mathbf{v}, t) |\mathbf{g} \cdot \hat{\boldsymbol{\sigma}}| (b_{\hat{\boldsymbol{\sigma}}} - 1) (v_x^2 + v_y^2). \quad (\text{A1})$$

By using the collision rule, Eqs. (1) and (2), it is

$$(b_{\hat{\boldsymbol{\sigma}}} - 1) (v_x^2 + v_y^2) = \left(\frac{m}{m+M} \right)^2 (1 + \alpha)^2 (\mathbf{g} \cdot \hat{\boldsymbol{\sigma}})^2 (\hat{\boldsymbol{\sigma}}_x^2 + \hat{\boldsymbol{\sigma}}_y^2) + \frac{2m}{m+M} (1 + \alpha) (\mathbf{g} \cdot \hat{\boldsymbol{\sigma}}) (v_x \hat{\boldsymbol{\sigma}}_x + v_y \hat{\boldsymbol{\sigma}}_y), \quad (\text{A2})$$

and \mathcal{G} can be expressed as

$$\mathcal{G} = \frac{\sigma^2}{2(h-\sigma)n} \left\{ \left(\frac{m}{m+M} \right)^2 (1 + \alpha)^2 \int_{\sigma/2}^{h-\sigma/2} dz \int_{\Sigma(z)} d\hat{\boldsymbol{\sigma}} G_1(\hat{\boldsymbol{\sigma}}) (\hat{\boldsymbol{\sigma}}_x^2 + \hat{\boldsymbol{\sigma}}_y^2) + \frac{2m}{m+M} (1 + \alpha) \int_{\sigma/2}^{h-\sigma/2} dz \int_{\Sigma(z)} d\hat{\boldsymbol{\sigma}} G_2(\hat{\boldsymbol{\sigma}}) \right\}, \quad (\text{A3})$$

where we have introduced

$$G_1(\hat{\boldsymbol{\sigma}}) = \int d\mathbf{v} \int d\mathbf{v}_1 f_1(\mathbf{v}_1) f(\mathbf{v}, t) |\mathbf{g} \cdot \hat{\boldsymbol{\sigma}}|^3, \quad (\text{A4})$$

$$G_2(\hat{\boldsymbol{\sigma}}) = \int d\mathbf{v} \int d\mathbf{v}_1 f_1(\mathbf{v}_1) f(\mathbf{v}, t) |\mathbf{g} \cdot \hat{\boldsymbol{\sigma}}| (\mathbf{g} \cdot \hat{\boldsymbol{\sigma}}) (v_x \hat{\boldsymbol{\sigma}}_x + v_y \hat{\boldsymbol{\sigma}}_y). \quad (\text{A5})$$

To evaluate the above integrals, it is convenient to use the following variables

$$\mathbf{c} = \frac{1}{\Omega} (v_x \mathbf{e}_x + v_y \mathbf{e}_y) + \frac{1}{\Omega_z} v_z \mathbf{e}_z, \quad (\text{A6})$$

$$\mathbf{c}_1 = \frac{1}{w} (v_{1x} \mathbf{e}_x + v_{1y} \mathbf{e}_y) + \frac{1}{w_z} v_{1z} \mathbf{e}_z. \quad (\text{A7})$$

Taking into account the Gaussian character of f_1 and f (see Eqs. (5) and (23)), it is obtained

$$G_1(\hat{\boldsymbol{\sigma}}) = \frac{n_1 n}{\pi^3} \int d\mathbf{X} e^{-X^2} |\mathbf{X} \cdot \mathbf{u}_a|^3 a^3, \quad (\text{A8})$$

$$G_2(\hat{\boldsymbol{\sigma}}) = \frac{n_1 n}{\pi^3} \int d\mathbf{X} e^{-X^2} |\mathbf{X} \cdot \mathbf{u}_a| (\mathbf{X} \cdot \mathbf{u}_a) a^2 (c_x \hat{\boldsymbol{\sigma}}_x + c_y \hat{\boldsymbol{\sigma}}_y), \quad (\text{A9})$$

where the time dependence in G_1 and G_2 has not been explicitly written because it comes entirely through the thermal velocities Ω and Ω_z . We have also introduced the six-dimensional variable $\mathbf{X} = (c_{1x}, c_{1y}, c_{1z}, c_x, c_y, c_z)$, the vector $\mathbf{a} = (w \hat{\boldsymbol{\sigma}}_x, w \hat{\boldsymbol{\sigma}}_y, w_z \hat{\boldsymbol{\sigma}}_z, -\Omega \hat{\boldsymbol{\sigma}}_x, -\Omega \hat{\boldsymbol{\sigma}}_y, -\Omega_z \hat{\boldsymbol{\sigma}}_z)$, its modulus $a \equiv |\mathbf{a}|$ and the unit vector $\mathbf{u}_a \equiv \mathbf{a}/a$. Performing the gaussian integrals and taking into account that $a = [(w^2 + \Omega^2)(\hat{\boldsymbol{\sigma}}_x^2 + \hat{\boldsymbol{\sigma}}_y^2) +$

$(w_z^2 + \Omega_z^2)\hat{\sigma}_z^2]^{1/2}$, it is obtained

$$G_1(\hat{\sigma}) = \frac{n_1 n}{\sqrt{\pi}} [(w^2 + \Omega^2)(\hat{\sigma}_x^2 + \hat{\sigma}_y^2) + (w_z^2 + \Omega_z^2)\hat{\sigma}_z^2]^{3/2},$$

$$G_2(\hat{\sigma}) = -\frac{n_1 n}{\sqrt{\pi}} \Omega^2 [(w^2 + \Omega^2)(\hat{\sigma}_x^2 + \hat{\sigma}_y^2) + (w_z^2 + \Omega_z^2)\hat{\sigma}_z^2]^{1/2} (\hat{\sigma}_x^2 + \hat{\sigma}_y^2).$$

To obtain the desired expression for \mathcal{G} , the above functions have to be inserted in Eq. (A3). Then, the relevant integrals to be performed are $\int_{\sigma/2}^{h-\sigma/2} dz \int_{\Sigma(z)} d\hat{\sigma} G_1(\hat{\sigma}) (\hat{\sigma}_x^2 + \hat{\sigma}_y^2)$ and $\int_{\sigma/2}^{h-\sigma/2} dz \int_{\Sigma(z)} d\hat{\sigma} G_2(\hat{\sigma})$. Performing the angular integration and introducing the dimensionless variables $y \equiv \frac{z-\frac{\sigma}{2}}{\sigma}$, the following result is obtained

$$\int_{\sigma/2}^{h-\sigma/2} dz \int_{\Sigma(z)} d\hat{\sigma} G_1(\hat{\sigma}) (\hat{\sigma}_x^2 + \hat{\sigma}_y^2) = 4\sqrt{\pi} n_1 n \sigma \int_0^\varepsilon dy (\varepsilon - y) (1 - y^2) [(w^2 + \Omega^2)(1 - y^2) + (w_z^2 + \Omega_z^2)y^2]^{3/2}, \quad (\text{A12})$$

$$\int_{\sigma/2}^{h-\sigma/2} dz \int_{\Sigma(z)} d\hat{\sigma} G_2(\hat{\sigma}) = -4\sqrt{\pi} n_1 n \sigma \Omega^2 \int_0^\varepsilon dy (\varepsilon - y) (1 - y^2) [(w^2 + \Omega^2)(1 - y^2) + (w_z^2 + \Omega_z^2)y^2]^{1/2}. \quad (\text{A13})$$

By inserting the above expressions in Eq. (A3), the expression of the main text, Eq. (30), is obtained.

- ¹A. Goldstein and M. Shapiro, *Mechanics of collisional motion of granular materials: Part I. General hydrodynamics equations*, J. Fluid Mech. **282**, 75 (1995).
- ²J. J. Brey, J. W. Dufty, C. S. Kim, and A. Santos, *Hydrodynamics for a granular flow at low density*, Phys. Rev. E **58**, 4638 (1998).
- ³I. Goldhirsch, *Rapid Granular Flows*, Annu. Rev. Fluid Mech. **35**, 57 (2003).
- ⁴I. S. Aranson and L. S. Tsimring, *Patterns and collective behavior in granular media: theoretical concepts*, Rev. Mod. Phys. **78**, 641 (2006).
- ⁵J. S. Olafsen and J. S. Urbach, *Clustering, Order, and Collapse in a Driven Granular Monolayer*, Phys. Rev. Lett. **81**, 4369 (1998).
- ⁶A. Prevost, D. A. Egolf, and J. S. Urbach, *Forcing and Velocity Correlations in a Vibrated Granular Monolayer*, Phys. Rev. Lett. **89**, 084301 (2002).
- ⁷K. Roeller, J. P. D. Clewett, R. M. Bowley, S. Herminghaus, and M. R. Swift, *Liquid-Gas Phase Separation in Confined Vibrated Dry Granular Matter*, Phys. Rev. Lett. **107**, 048002 (2011).
- ⁸J. P. D. Clewett, K. Roeller, R. M. Bowley, S. Herminghaus, and M. R. Swift, *Emergent Surface Tension in Vibrated, Noncohesive Granular Media*, Phys. Rev. Lett. **109**, 228002 (2012).
- ⁹P. Melby, F. Vega Reyes, A. Prevost, R. Robertson, P. Kumar, D. A. Egolf, and J. S. Urbach, *The dynamics of thin vibrated granular layers*, J. Phys.: Condens. Matter **17** (2005) S2689-S2704.
- ¹⁰J. S. Olafsen and J. S. Urbach, *Two-Dimensional Melting Far from Equilibrium in a Granular Monolayer*, Phys. Rev. Lett. **95**, 098002 (2005).

- ¹¹G. Gradenigo, A. Sarracino, D. Villamaina, and A. Puglisi, *Nonequilibrium length in granular fluids: From experiment to fluctuating hydrodynamics*, EPL **96** (2011) 14004.
- ¹²A. Puglisi, A. Gnoli, G. Gradenigo, A. Sarracino, and D. Villamaina, *Structure factors in granular experiments with homogeneous fluidization*, J. Chem. Phys. **136**, 014704 (2012).
- ¹³J. Castillo, N. Mújica, and R. Soto, *Fluctuations and Criticality of a Granular Solid-Liquid-Like Phase Transition*, Phys. Rev. Lett. **109**, 095701 (2012).
- ¹⁴M. Guzmán and R. Soto, *Critical phenomena in quasi-two-dimensional vibrated granular systems*, Phys. Rev. E **97**, 012907 (2018).
- ¹⁵R. Brito, D. Risso, and R. Soto, *Hydrodynamic modes in a confined granular fluid*, Phys. Rev. E **87**, 022209 (2013).
- ¹⁶J. J. Brey, M. I. García de Soria, and P. Maynar, *Homogeneous steady state of a confined granular gas*, Phys. Rev. E **88**, 062205 (2013).
- ¹⁷R. Soto, D. Risso, and R. Brito, *Shear viscosity of a model for confined granular media*, Phys. Rev. E **90**, 062204 (2014).
- ¹⁸J. J. Brey, P. Maynar, M. I. García de Soria, and V. Buzón, *Homogeneous hydrodynamics of a collisional model of confined granular gases*, Phys. Rev. E **89**, 052209 (2014).
- ¹⁹J. J. Brey, M. I. García de Soria, P. Maynar, and V. Buzón, *Memory effects in the relaxation of a confined granular gas*, Phys. Rev. E **90**, 032207 (2014).
- ²⁰J. J. Brey, V. Buzón, P. Maynar, and M. I. García de Soria, *Hydrodynamics for a model of a confined quasi-two-dimensional granular gas*, Phys. Rev. E **91**, 052201 (2015).
- ²¹J. J. Brey, V. Buzón, M. I. García de Soria, and P. Maynar, *Stability analysis of the homogeneous hydrodynamics of a model for a confined granular gas*, Phys. Rev. E **93**, 062907 (2016).
- ²²D. Risso, R. Soto, and M. Guzmán, *Effective two-dimensional model for granular matter with phase separation*, Phys. Rev. E **98**, 022901 (2018).
- ²³P. Maynar, M. I. García de Soria, and J. J. Brey, *Homogeneous dynamics in a vibrated granular monolayer*, J. Stat. Mech. (2019) 093205.
- ²⁴P. Maynar, M. I. García de Soria, and J. J. Brey, *Understanding an instability in vibrated granular monolayers*, Phys. Rev. E **99**, 032903 (2019).
- ²⁵N. Rivas, S. Ponce, B. Gallet, D. Risso, R. Soto, P. Cordero, and N. Mújica, *Sudden Chain Energy Transfer Events in Vibrated Granular Media*, Phys. Rev. Lett. **106**, 088001 (2011).
- ²⁶N. Rivas, P. Cordero, D. Risso, and R. Soto, *Characterization of the energy burst in vibrated shallow granular systems*, Granular Matter (2012) 14:157-162.
- ²⁷V. Buzón Díaz, *Estudio de un modelo cinético de gas granular confinado*, PhD thesis, Universidad de Granada (2017).
- ²⁸J. J. Brey, P. Maynar, and M. I. García de Soria, *Kinetic equation and nonequilibrium entropy for a quasi-two-dimensional gas*, Phys. Rev. E **94**, 040103 (2016).
- ²⁹J. J. Brey, M. I. García de Soria, and P. Maynar, *Boltzmann kinetic equation for a strongly confined gas of hard spheres*, Phys. Rev. E **96**, 042117 (2017).
- ³⁰J. J. Brey, M. I. García de Soria, and P. Maynar, *Self-diffusion in a quasi-two-dimensional gas of hard spheres*, Phys. Rev. E **101**, 012102 (2020).
- ³¹J. R. Dorfman and H. van Beijeren, *The Kinetic Theory of Gases*. In *Statistical Mechanics, Part B*, ed. B. J. Berne (Plenum Press, New York, 1977).
- ³²J. J. Brey and M. J. Ruiz-Montero, *Vibrated granular gas confined by a piston*, Phys. Rev. E **79**, 031305 (2009).
- ³³J. J. Brey, J. W. Dufty, and A. Santos, *Kinetic Models for Granular Flow*, J. Stat. Phys. **97**, 281 (1999).
- ³⁴A. Santos and J. W. Dufty, *Critical Behavior of a Heavy Particle in a Granular Fluid*, Phys. Rev. Lett. **86**, 4823 (2001).
- ³⁵A. Santos and J. W. Dufty, *Nonequilibrium phase transition for a heavy particle in a granular fluid*, Phys. Rev. E **64**, 051305 (2001).
- ³⁶M. P. Allen and D. J. Tisdley, *Computer Simulations of Liquids* (Oxford Science Publications, New York, 1987).
- ³⁷M. I. García de Soria, P. Maynar, and J. J. Brey, *Critical behavior of an intruder in a quasi-two-dimensional vibrated granular gas*, to be published.